Journal of MATERIALS RESEARCH

Article
DOI:10.1557/s43578-021-00119-3

ADVANCED NANOMECHANICAL TESTING

FOCUS ISSUE

Contact area correction for surface tilt in pyramidal nanoindentation

Joseph E. Jakes[1,a], Douglas Stauffer[2]

[1] Forest Biopolymers Science and Engineering, Forest Products Laboratory, USDA Forest Service, One Gifford Pinchot Drive, Madison, WI 53726, USA

[2] Hysitron Product Line, Bruker Nano Surfaces & Metrology, 9625 West 76th St, Eden Prairie, MN 55419, USA

[a] Address all correspondence to this author. e-mail: joseph.e.jakes@usda.gov

Received: 12 November 2020; accepted: 26 January 2021; published online: 12 February 2021

A correction is needed to minimize errors in contact area caused by surface tilt in nanoindentation. Surface tilt decreases the contact area calculated using standard analyses that assume the tested surface is not tilted and thus results in overestimation of hardness and elastic modulus. Both the direction of tilt with respect to the pyramid face and the angle of the pyramidal probe are important when characterizing error caused by surface tilt. Here, a geometric model was used to create contour plots from which the area correction factor can be directly determined using only the ratios of side lengths measured from an image of the triangular nanoindentation impression. Contour plots for Berkovich, cube corner, and two nonstandard pyramidal probe geometries are given. The efficacy of the method was demonstrated in the correction of Berkovich nanoindentation on facets in freshly prepared poly(methyl methacrylate) with surface tilts as high as 6°.

Introduction

Nanoindentation is a popular technique used to assess mechanical properties in a wide variety of materials, including metals, ceramics, polymers, and biological tissues, and is especially useful for its ability to probe properties at small length scales. In nanoindentation, a carefully shaped probe is pressed into and withdrawn from a material following a prescribed loading function. During the experiment, both load and displacement are continuously measured, and from the resulting load–depth trace, mechanical properties can be assessed, including indentation hardness

$$H = \frac{P_0}{A_0}, \tag{1}$$

where P_0 and A_0 are maximum load and projected contact area immediately prior to unloading, respectively, and the effective modulus of contact

$$E_{\mathrm{eff}} = \frac{S}{A_0^{1/2}}, \tag{2}$$

where S is contact stiffness attributable to the material and indenter probe calculated at the slope of the initial unloading. For indentation against a homogenous, isotropic, elastic half-space,

$$\frac{1}{E_{\mathrm{eff}}} = \frac{\pi^{1/2}}{2\beta}\left(\frac{1-\nu_s^2}{E_s} + \frac{1-\nu_d^2}{E_d}\right), \tag{3}$$

where E_s is the indentation modulus of the specimen, E_d is Young's modulus of the indenter, and ν_s and ν_d are Poisson's ratios of specimen and indenter, respectively. β is a numerical factor that is often assumed to be 1, but its numerical value is debated [1–5]. For the analyses in this paper, $\beta = 1$ is assumed. Pyramidal probes are often used in nanoindentation, with the three-sided Berkovich probe [6] being one of the most common. For Berkovich nanoindentation, A_0 in Eqs. 1 and 2 can be assessed from the load–depth trace using a probe area function and the Oliver–Pharr contact depth [7]

$$h_c = h_0 - 0.75\frac{P_0}{S}, \tag{4}$$

where h_0 is depth immediately prior to unloading. The probe area function is calculated using a series of nanoindentations in a calibration material with known properties, most often fused silica [7, 8].

Surface tilt is one of many well-known experimental factors that can cause errors in nanoindentation results [8–14]. In an ideal indentation experiment, the probe axis of symmetry is parallel to the loading direction and perpendicular to the flat specimen surface. From geometry, any deviation from perpendicularity of the probe axis of symmetry with the flat specimen surface results in an underestimated A_0 when A_0 is calculated using depth [8–14]. An underestimated A_0 will result in an overestimated H and E_s. The overestimation will be larger in H than E_s because H depends on A_0, whereas E_s depends on ${A_0}^{1/2}$. For a given pyramidal probe, the magnitude of the A_0 error caused by surface tilt depends on both the angle of the surface tilt and the tilt direction with respect to the pyramid edge or face. The effect is larger when the surface is tilted up towards an edge. For a given surface tilt, the magnitude of the A_0 error is higher for blunter pyramidal probes than sharper. For instance, the error for a Berkovich probe would be higher than for a cube corner probe. Using pyramidal probes with a wide range of probe angles, including those blunter than a Berkovich probe, to measure different stress states and other unique properties attracts considerable interest [15–17]. Therefore, corrections are needed to minimize systematic contact area errors caused by using probes with different angles in a tilted surface.

In addition to underestimating A_0, horizontal compliance of the indenter stem [12] and changes in the plastic strain field [9] may also affect the nanoindentation measurement in a tilted surface. However, simulated nanoindentation experiments in surfaces with tilts up to 5° reveal that these other factors are relatively minor and accurate nanoindentation H and E_s can be obtained by using the actual contact areas in the tilted surface planes [9, 12, 14].

A few theoretical models have been developed to geometrically correct A_0 for surface tilt, but they all have shortcomings because they either are only valid for small surface tilts, require difficult-to-measure parameters, or do not consider the actual contact area of interest. Oliver and Pharr developed a method to correct Berkovich nanoindentation areas for surface tilt using a ratio of the longest side length to the shortest side length measured from an image of the residual nanoindentation [8], but the method is useful only for surface tilts less than about 2°. Kashani and Madhavan developed models to calculate geometric area correction factors for surface tilt for Berkovich, cube corner, and conical probes [11, 12]. However, the correction method requires a priori knowledge of both surface tilt and how the tilt is oriented with respect to pyramid edge or face, parameters that are not readily measured experimentally because of the need to account for scanner nonlinearities. Additionally, their correction factor was calculated using the area projected on the plane perpendicular to the probe axis of symmetry, not the plane of the specimen surface, which would be the actual contact area of interest. Despite this, Huang et al. [13] used Kashani and Madhavan's models to develop a method using ratios of the contact edge lengths measured from images of residual indent impressions to calculate the surface tilt and angle defining how the surface is tilted with respect to the pyramid edge or face, which could then be used to calculate the geometric area correction factor.

The aim of the present work is to provide contour plots from which geometric area correction factors can be directly read for a triangular pyramid probe. The actual contact area in the specimen surface plane will be used in the model to create the contour plots. The only experimental inputs needed to use the contour plots will be the three side lengths measured from a two-dimensional image of the triangular nanoindentation impression. Contour plots will be created for Berkovich, cube corner, and two nonstandard triangular pyramid probes. The utility of the method will be demonstrated experimentally by comparing uncorrected and tilt-corrected H and E_s from Berkovich nanoindentations in poly(methyl methacrylate) (PMMA) surfaces with surface tilts up to 6°. In addition to providing area correction factors, the contour plots can also be useful to estimate the unknown surface tilt angle of the tested surface.

Theory

To create a model for correcting nanoindentation contact areas for surface tilt, a pyramidal probe is represented as a regular triangular pyramid placed in a Cartesian coordinate system (Fig. 1a and c) with its apex at coordinate (0, 0, 0), vertical axis along the z-axis, and three edges defined by the vectors

$$\boldsymbol{E}_1 = \left(-\tan\theta, \frac{3\tan\theta}{\sqrt{3}}, 1\right) \tag{5}$$

$$\boldsymbol{E}_2 = \left(-\tan\theta, -\frac{3\tan\theta}{\sqrt{3}}, 1\right) \tag{6}$$

$$\boldsymbol{E}_3 = (2\tan\theta, 0, 1) \tag{7}$$

where θ is the angle from the z-axis to the pyramid face. The contact area is defined as the area intersected by the triangular pyramid and a plane representing the specimen surface that passes through the coordinate (0, 0, 1) and is defined by the normal vector

$$\boldsymbol{n} = (x, y, 1) = (\tan(\varphi)\cos(\psi), \tan(\varphi)\sin(\psi), 1) \tag{8}$$

where φ is the surface tilt angle with respect to the z-axis and ψ is the angle defining the rotation of the surface tilt about the z-axis with respect to a pyramid face ($\psi = 0°$) or edge ($\psi = 60°$) (Fig. 1b and d). Using the coordinate (0, 0, 1) and $\boldsymbol{n}$, the plane equation is

$$\tan(\varphi)\cos(\psi)x + \tan(\varphi)\sin(\psi)y + (z - 1) = 0 \tag{9}$$

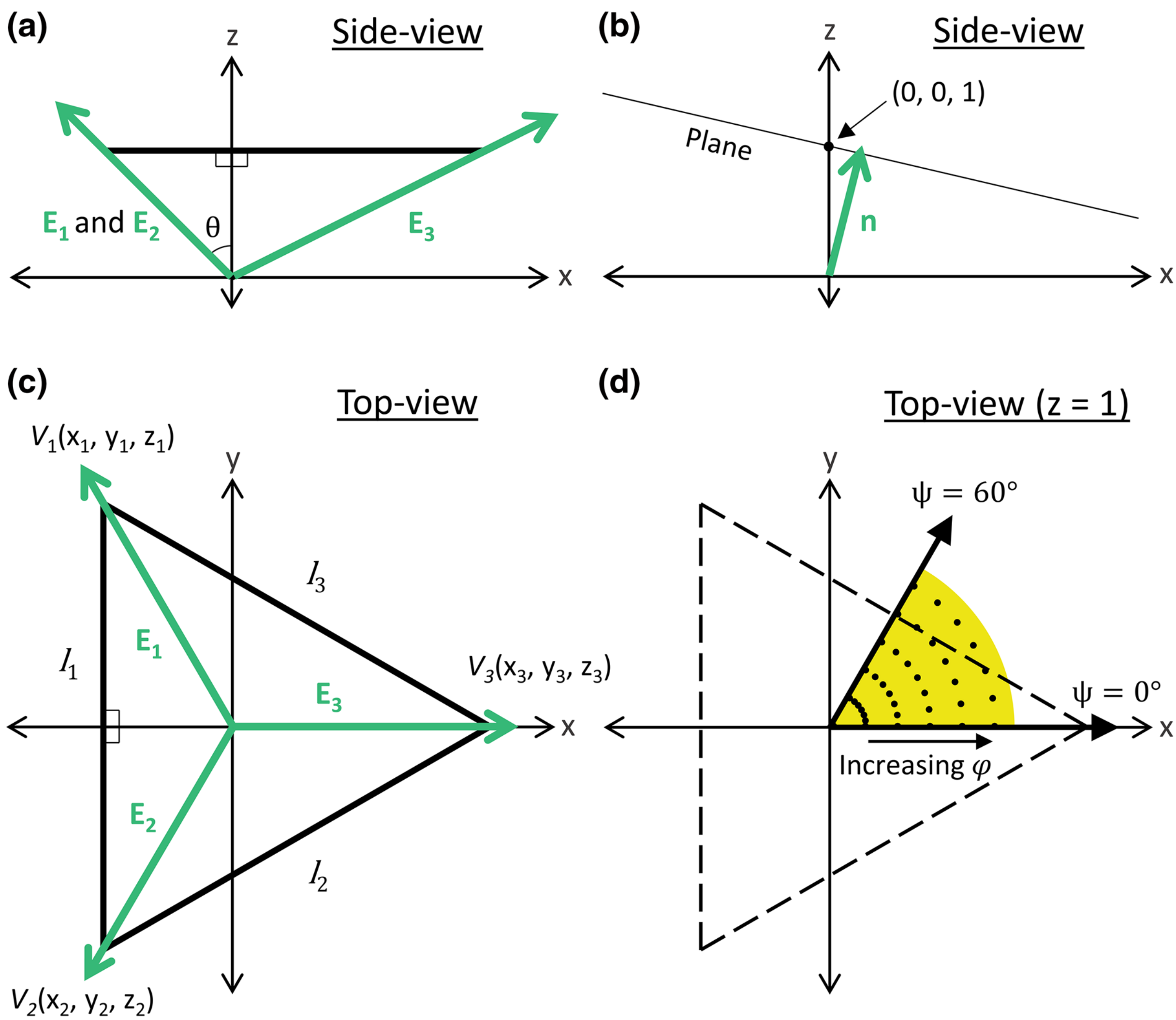

Figure 1: (a) and (c) Triangular pyramid defined in the cartesian coordinate system. The triangle side length labels (l_1, l_2, and l_3) and vertex labels (V_1, V_2, and V_3) are shown in (c). (b) and (d) Illustration of how series of tilted planes defined by a normal vector **n** and coordinate (0,0,1) were defined for calculating contact areas as a function of surface tilt. The dots in (d) are representative of points in the z = 1 plane that were used to define ***n*** over a wide range of surface tilts. The arches of dots equidistant from the x–y origin define series of planes at the same tilt angle (φ) but towards a pyramid edge ($\psi = 60°$), pyramid face ($\psi = 0°$), or in between ($0° < \psi < 60°$). The sets of points in a line that intersects the x–y origin define a series of planes tilted with different φ, but a constant ψ.

Because of probe symmetry, only values of $0° < \psi < 60°$ need to be included in the model. Additionally, because ideal pyramidal probes are self-similar, only the single set of planes through (0, 0, 1) needs to be included.

The coordinates at which the three edge vectors (Eqs. 5–7) intersect the plane (Eq. 9) define the area intersected by the triangular pyramid and plane. Parametric equations can be used to calculate these coordinates. Equations 5–7 can be represented as

$$\boldsymbol{E_i} = (a_i, b_i, c_i,), \tag{10}$$

where $i = 1$, 2, or 3, and a_i, b_i, and c_i are the corresponding expressions in Eqs. 5–7. Then the parametric equations are given by

$$x_i = a_i t_i \tag{11}$$

$$y_i = b_i t_i \tag{12}$$

$$z_i = c_i t_i \tag{13}$$

Substituting Eqs. 11–13 into the plane equation (Eq. 9) and solving for t_i gives

$$t_i = \frac{1}{\tan(\varphi)\cos(\psi)a_i + \tan(\varphi)\sin(\psi)b_i + c_i} \tag{14}$$

The edge intersection coordinates for each vertex $V_i(x_i, y_i, z_i)$ can then be calculated by substituting Eq. 14 into Eqs. 11–13. Two-dimensional projections on the x–y plane for series of areas intersected by tilted planes and a Berkovich probe ($\theta = 65.27°$) are shown in Fig. 2 as a function of φ and ψ. From visual observation, for a given φ the contact area depends strongly on the direction of surface tilt with respect to the edge or face of the probe, with the surface tilting up towards an edge ($\psi = 60°$) having much larger areas than tilts up towards a face ($\psi = 0°$).

Calculating the area intersected by the defined plane and pyramid is accomplished by first calculating the triangle side lengths in the specimen surface plane using

$$l_1 = \left((x_1 - x_2)^2 + (y_1 - y_2)^2 + (z_1 - z_2)^2\right)^{1/2} \quad (15)$$

$$l_2 = \left((x_2 - x_3)^2 + (y_2 - y_3)^2 + (z_2 - z_3)^2\right)^{1/2} \quad (16)$$

$$l_3 = \left((x_3 - x_1)^2 + (y_3 - y_1)^2 + (z_3 - z_1)^2\right)^{1/2} \quad (17)$$

Then the area A is calculated using Heron's formula [18]

$$A = \left(p(p - l_1)(p - l_2)(p - l_3)\right)^{1/2} \quad (18)$$

where

$$p = \frac{l_1 + l_2 + l_3}{2} \quad (19)$$

An area correction factor $\mathcal{A}$ is defined using

$$\mathcal{A} = \frac{A}{A_\perp} \quad (20)$$

where $A_\perp$ is the area for a perpendicular surface at $\varphi = 0°$. Figure 3 shows $\mathcal{A}$ as a function of surface tilt φ for values of ψ = 0° and 60°. $\mathcal{A}$ is greater than one because A in a tilted surface is always larger than $A_\perp$. The figure includes data for the

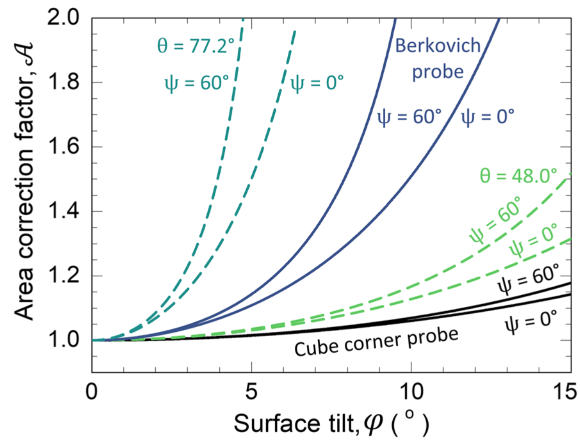

Figure 3: Area correction factor ($\mathcal{A}$) as a function of surface tilt (φ) for θ = 77.2°, Berkovich (θ = 65.27°), θ = 48.0°, and cube corner (θ = 35.28°) pyramidal probes. For each probe, $\mathcal{A}$ is plotted for tilt up towards a pyramid edge (ψ = 60°) and up towards a pyramid face (ψ = 0°).

Berkovich probe (θ = 65.27°), cube corner probe (θ = 35.28°), and two other pyramidal geometries (θ = 48.0° and 77.2°). The effects of surface tilt are much larger for blunter probes, 77.2° having a larger $\mathcal{A}$ than the Berkovich, and so on, with the cube corner probe having the smallest $\mathcal{A}$. For example, at φ = 2° the cube corner has a negligible $\mathcal{A}$, whereas the Berkovich and θ = 77.2° have $\mathcal{A}$ values of 1.02 and 1.08, respectively. For a given probe and φ, the $\mathcal{A}$ values are larger for tilt towards an edge (ψ = 60°) than towards a face (ψ = 0°). Experimentally, the corrected contact area A_0^c can be calculated using

$$A_0^c = \mathcal{A} A_o \quad (21)$$

Finally, A_0^c can then be substituted for A_0 in Eqs. 1 and 2 to calculate tilt-corrected H and E_{eff}, respectively.

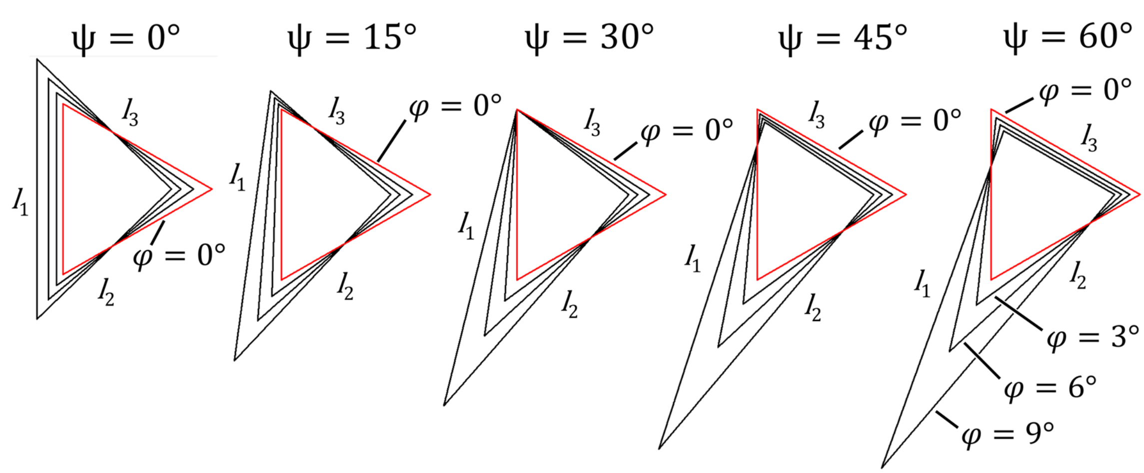

Figure 2: Series of two-dimensional areas projected to the x–y plane defined by the intersections of tilting planes (Eq. 9) and a Berkovich probe (θ = 65.27°). For each value of ψ, which defines the direction of the surface tilt (φ) with respect to tilt up to a pyramid face (ψ = 0°) or edge (ψ = 60°), areas are plotted for φ = 0°, 3°, 6°, and 9°.

However, a plot like Fig. 3 cannot be readily used to correct experimental data because φ and ψ are usually not known for a given experiment. Fortunately, side lengths measured from an image of a residual nanoindentation impression can be used. Such images could be collected using various types of microscopy, including scanning probe microscopy, optical microscopy, or scanning electron microscopy. Measuring side length in the specimen surface plane using scanning probe microscopy is possible. However, more easily and more likely obtained are side length measurements using a two-dimensional image. Therefore, side lengths in two dimensions will be used in our model. The side lengths projected into the x–y plane can be calculated using

$$l_1^{XY} = \left((x_1 - x_2)^2 + (y_1 - y_2)^2\right)^{1/2} \tag{22}$$

$$l_2^{XY} = \left((x_2 - x_3)^2 + (y_2 - y_3)^2\right)^{1/2} \tag{23}$$

$$l_3^{XY} = \left((x_3 - x_1)^2 + (y_3 - y_1)^2\right)^{1/2} \tag{24}$$

Using the subscript labels indicated in Figs. 1 and 2, for 0° < ψ < 60°, the relationships $l_1^{XY} > l_2^{XY} > l_3^{XY}$ will always hold except when ψ = 0° or 60°, and the intersected area will be an isosceles triangle. Then $l_2^{XY} = l_3^{XY}$ or $l_1^{XY} = l_2^{XY}$ when ψ = 0° or 60°, respectively.

Oliver and Pharr suggested determining an area correction factor for small surface tilts based on the ratio of the longest side length (l_l) to the shortest side length (l_s) [8]. For our model, l_1^{XY}/l_3^{XY} equals l_l/l_s. Figure 4 shows $\mathcal{A}$ as a function of l_l/l_s and ψ for a Berkovich probe. The problem with using only l_l/l_s to calculate $\mathcal{A}$ is that for a given l_l/l_s, $\mathcal{A}$ is not a unique value because it depends on ψ. For example, at $l_l/l_s = 1.2$, which may correspond to a surface tilt as small as 3°, $\mathcal{A}$ ranges from 1.03 or 1.07 depending on ψ. Calculating $\mathcal{A}$ using only l_l/l_s is not reliable for surface tilts greater than about 2°.

To more accurately determine $\mathcal{A}$ for surfaces with tilts larger than 2°, the ratio of the longest side length to the side with the middle length (l_m) will also be used, which in our model is $l_l/l_m = l_1^{XY}/l_2^{XY}$. Figure 5 shows l_l/l_s and l_l/l_m as functions of tilt for a Berkovich probe. Note that over the range of surface tilts plotted in Fig. 5, a given value of l_l/l_m is not always a unique function of surface tilt, whereas l_l/l_s is always a unique function of surface tilt. Therefore, our approach for using both l_l/l_s and l_l/l_m to determine $\mathcal{A}$ is to numerically calculate $\mathcal{A}$ as a function of l_l/l_m for chosen values of l_l/l_s. This results in a series of l_l/l_s contours as plotted in Fig. 6a and b for Berkovich and cube corner probes, respectively. To correct experimental nanoindentations, the three side lengths of a triangular nanoindentation impression can be measured to determine l_l/l_s and l_l/l_m. Then the contour plot corresponding to the appropriate probe can be used to determine $\mathcal{A}$ for use in Eq. 21 to calculate A_0^c.

As previously noted, and shown in Fig. 3, as a function of surface tilt the magnitude of $\mathcal{A}$ is much higher for blunter probes like the Berkovich than for sharper probes like the cube corner. In contrast, for given values of l_l/l_m and l_l/l_s, $\mathcal{A}$ is higher for sharper probes than blunter probes (Fig. 6). Therefore, separate $\mathcal{A}$ contour plots are needed for pyramidal probes with different θ angles. Additional contour plots spanning wider ranges of side length ratios, as well as for pyramidal probes with θ = 48.0° and 77.2°, are provided in the Supplementary Information. The surface tilt angle φ contours in Fig. 6 can also be used to estimate an

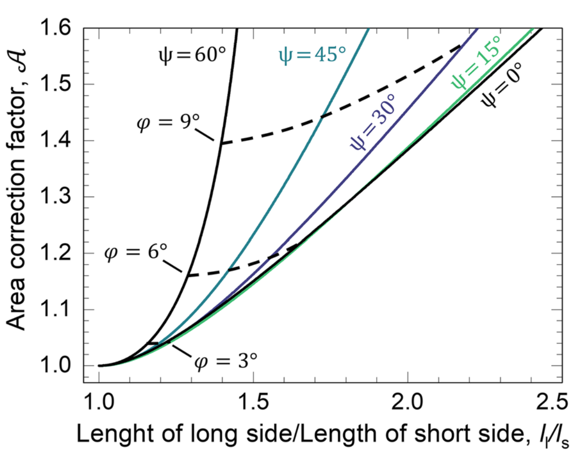

Figure 4: Area correction factor ($\mathcal{A}$) as a function of triangle side length ratio of the length of the longest side to the length of the shortest side (l_l/l_s) for a Berkovich probe (θ = 65.27°). $\mathcal{A}$ is plotted for tilt up towards a pyramid edge (ψ = 60°), up towards a pyramid face (ψ = 0°), and 15° intervals in between. The surface tilt (φ) angles are also indicated as dashed lines.

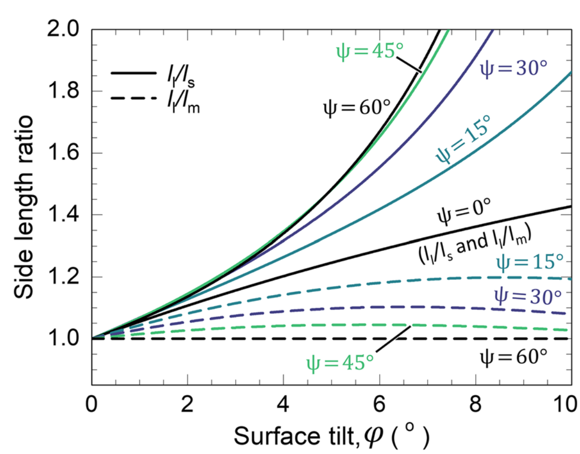

Figure 5: Triangle side length ratios of the length of the longest side to the length of the medium side (l_l/l_m) and length of the longest side to the length of the shortest side (l_l/l_s) as functions of surface tilt (φ). For both tilt up towards a pyramid face (ψ = 0°) and up towards a pyramid edge (ψ = 60°), the nanoindentation impression is an isosceles triangle with $l_s = l_m$ and $l_l = l_m$, respectively.

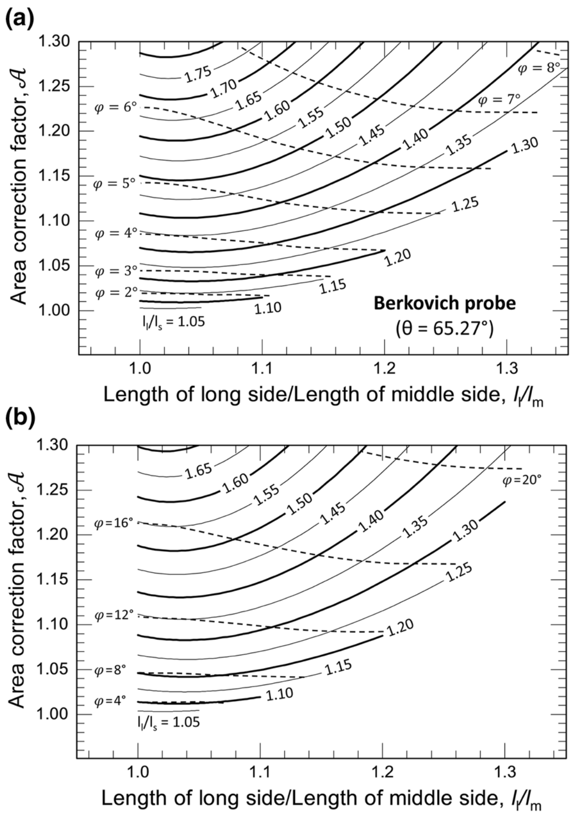

Figure 6: Area correction factor ($\mathcal{A}$) contour plots for (a) Berkovich ($\theta = 65.27°$) and (b) cube corner ($\theta = 35.28°$) probes. The $\mathcal{A}$ can be determined using the ratios of the longest side length to medium side length (l_l/l_m) and longest side length to shortest side length (l_l/l_s). The l_l/l_m is plotted on the abscissa and the l_l/l_s values follow the solid line contours. The surface tilt (φ) angles are indicated as dashed line contours.

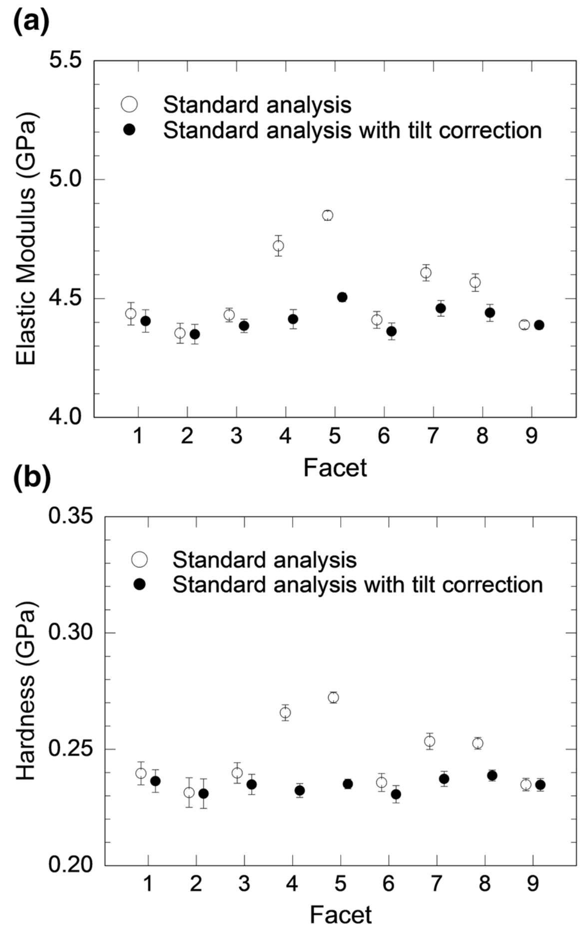

Figure 7: Average PMMA (a) elastic modulus and (b) hardness for nanoindentation series performed in each of the nine prepared facets. Error bars are standard deviations.

unknown φ of a tested specimen surface. For measuring φ based on side length ratios, blunter probes provide more sensitivity.

Experimental results and discussion

To test the efficacy of the developed contact area correction method, series of Berkovich nanoindentations with loads from 1 to 12 mN were placed in facets prepared in PMMA with surface tilts as high as 6°. No size dependence in elastic modulus or hardness was observed within a series of nanoindentations on a given facet, which agrees with the previous results for freshly prepared PMMA surfaces in this material [19]. Therefore, the property values were averaged for each of the nine facets (Fig. 7). Using the standard analysis without a surface tilt correction, the calculated average indentation modulus (E_s) and indentation hardness (H) varied from 4.4 to 4.9 GPa and 0.23 to 0.27 GPa, respectively. These property values are consistent with literature quasistatic Berkovich probe nanoindentation results [20–22]. However, the differences in E_s and H between facets were not expected to be real. The facets with the higher property values were likely affected by errors caused by surface tilt.

To apply the geometric area correction, measurements of the nanoindentation impression side lengths are needed. Such measurements were made using atomic force microscopy (AFM) images of residual nanoindentations (Fig. 8). The three side lengths were measured for each nanoindentation by drawing straight lines between the vertices. Then the l_l/l_s and l_l/l_m ratios were calculated. The side length ratios were independent of size within a series of nanoindentations on a given facet. Therefore, the same $\mathcal{A}$ (Fig. 6a) was applied to all the nanoindentations on a given facet. The property values corrected for surface tilt are also plotted in Fig. 7, with the calculated average E_s and H now varying from 4.4 to 4.5 GPa and 0.23 to 0.24 GPa, respectively. Indeed, facets 4 and 5, which had the highest property values in the standard analysis, were the most affected by surface tilt, with $\mathcal{A}$ values of 1.14 and 1.16, respectively. Evidently, applying the geometric area correction factor $\mathcal{A}$ to experiments in surfaces with tilts as high as 6° was all that was needed to obtain H and E_s

Journal of Materials Research ■ Volume 36 ■ Issue 11 ■ June 2021 ■ www.mrs.org/jmr

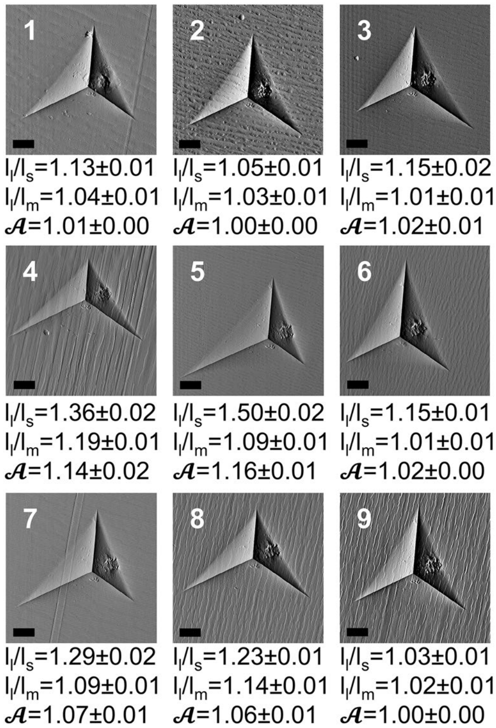

Figure 8: Atomic force microscopy (AFM) images of 12 mN nanoindentation impressions placed on each of the nine PMMA facets. For each nanoindentation, the ratio of longest side length to shortest side length (l_l/l_s), ratio of the longest side length to medium side length (l_l/l_m), and area correction factor ($\mathcal{A}$) determined from Fig. 6a are given. The side length ratios are the averages from the nine nanoindentations in each series, and the side length ratio uncertainties are 95% confidence intervals calculated by multiplying the standard error by 1.96. The $\mathcal{A}$ uncertainties represent the ranges of $\mathcal{A}$ determined from Fig. 6a using the range of side length ratios encompassed by their uncertainties. Scale bars are 2 μm.

values that agree with the values obtained in the surfaces without tilt. This is in agreement with the previous simulation results showing that accurate nanoindentation results can be obtained in surfaces with tilts up to 5° by simply using the actual contact areas in the surface planes [9, 12, 14].

Although in principle this contact area correction can be applied to nanoindentation in surfaces with tilts much higher than 6°, some caution is advised. It is likely that nanoindentation in highly tilted surfaces will be more affected by the horizontal compliance of the indenter stem [12] and changes in the plastic strain field [9]. It is also unclear how the validity of the Sneddon relationships [23] implicit in the nanoindentation analysis may be affected at larger surface tilts. Surface tilt may also affect the numerous correction factors that are often used to improve the accuracy of nanoindentation, such as the lateral displacement corrections for contact area [5], the variable epsilon factor [5], and the numerical factor β [1–4]. It is also unclear how well the geometric correction factor would work for nanoindentations with pile-up. The PMMA nanoindentations used to demonstrate the effectiveness of the geometric correction factor did not exhibit any obvious pile-up (Fig. 8). The geometric correction factor may not work as well if the pile-up behavior is affected by surface tilt and different sides of the triangular nanoindentation impression have different amounts of pile-up. The presented correction method only applies a geometric correction for the calculated contact area and does not address these other issues.

Conclusions

A simple-to-implement method was developed to correct nanoindentation contact areas for geometric errors caused by surface tilt. Contour plots were created in which $\mathcal{A}$ is given as a function of l_l/l_m and l_l/l_s for Berkovich, cube corner, and two nonstandard pyramidal probes (θ = 48.0° and 77.2°). For a given nanoindentation, the $\mathcal{A}$ is determined from the contour plot using l_l/l_m and l_l/l_s calculated from side lengths measured from a two-dimensional image of the residual nanoindentation impression. The $\mathcal{A}$ is then used to correct the A_0 calculated in the standard analysis. Finally, the corrected A_0 is used to calculate the tilt-corrected H and E_s. The effectiveness of the correction method was demonstrated by successfully correcting nanoindentation H and E_s measurements on PMMA facets with surface tilts as high as 6°.

Experimental methods

The poly(methyl methacrylate) (PMMA) specimen was taken from a 3.33-mm-diameter extruded rod (density 1.15 g/cm^3) obtained from Cope Plastics, Inc. (Godfrey, Illinois, USA). A 5-mm-tall cylinder was cut from the rod, and one end was bonded to the end of a metal cylinder with epoxy. The metal cylinder was fitted into a Leica EM UC7 ultramicrotome (Wetzlar, Germany) equipped with a diamond knife. Nine facets for nanoindentation experiments were prepared in different directions with surface tilts up to 6°. Experiments were performed using a Bruker-Hysitron (Minneapolis, Minnesota, USA) TriboIndenter® equipped with a Berkovich probe. The machine compliance, tip roundness effects, and probe area function were determined from a series of 120 nanoindents in a fused silica standard using a previously established load function and procedure [24]. Following the prescribed calibration reporting procedure [24], values for the square root of the Joslin–Oliver parameter of 1.219 ± 0.001 μm/N$^{1/2}$, elastic modulus of 72.1 ± 0.1 GPa, and Meyer's hardness of 9.19 ± 0.02 GPa (uncertainties are standard errors) were assessed for fused silica calibration nanoindentations with contact depths between 33 and 211 nm; no systematic variations of machine compliance or Joslin–Oliver parameter were observed in the systematic SYS plot analysis over this range of contact depths. The nanoindentation numerical correction factor β = 1 was used in the calibrations and experiments. The ideal 24.5 value for a Berkovich probe was used for the lead coefficient in the probe area function.

A series of nine load-control nanoindentations with maximum loads from 1 to 12 mN were placed in each facet. The load function consisted of a 5-s load, 5-s hold at maximum load, 2-s unload to 40% of the maximum load, 60-s thermal drift segment at 40% of maximum load, and finally a 1-s unload. The thermal drift was measured from the final 30 s of the thermal drift segment and used to correct the depth of penetration. The standard method was used to assess elastic modulus and hardness [7, 8]. The initial unloading stiffness of each unloading segment was assessed by fitting a power law function [7] to 40–98% of the maximum load in the unloading segment. The PMMA elastic modulus was calculated using a PMMA Poisson's ratio of 0.37 [25], and a diamond probe elastic modulus and Poisson's ratio of 1137 GPa and 0.07, respectively.

A Quesant (Agoura Hills, California, USA) atomic force microscope incorporated in the TriboIndenter was used to image the residual nanoindentation impressions. The AFM was operated in contact mode and calibrated in the lateral directions using an Advanced Surface Microscopy (Indianapolis, Indiana, USA) calibration standard as described previously [4]. The collected AFM images measured 15 µm in the horizontal and vertical directions and had a resolution of 40 pixels/µm in both directions. Side lengths of the residual nanoindentation impressions were measured using FIJI [26].

Acknowledgments

The authors acknowledge Bernie Becker for helpful discussion and verification on the theory.

Data availability

Data can be available upon reasonable request to the corresponding author.

Compliance with ethical standards

Conflict of interest On behalf of all authors, the corresponding author states that there is no conflict of interest.

Supplementary Information

The online version of this article (https://doi.org/10.1557/s43578-021-00119-3) contains supplementary material, which is available to authorized users.

References

1. R.B. King, Elastic analysis of some punch problems for a layered medium. Int. J. Solids Struct. **23**(12), 1657 (1987)
2. J.H. Strader, S. Shim, H. Bei, W.C. Oliver, G.M. Pharr, An experimental evaluation of the constant β relating the contact stiffness to the contact area in nanoindentation. Philos. Mag. **86**(33), 5285 (2006)
3. A. Bolshakov and G. M. Pharr: Inaccuracies in Sneddon's solution for elastic indentation by a rigid cone and their implications for nanoindentation data analysis, in Thin Films: Stresses and Mechanical Properties VI, edited by W. W. Gerberich, H. Gao, J.-E. Sundgren, and S. P. Baker (Mater. Res. Soc. Symp. Proc. 436, San Francisco, CA, USA, 1997), p. 189.
4. J.E. Jakes, C.R. Frihart, J.F. Beecher, R.J. Moon, D.S. Stone, Experimental method to account for structural compliance in nanoindentation measurements. J. Mater. Res. **23**(4), 1113 (2008)
5. T. Chudoba, N.M. Jennett, Higher accuracy analysis of instrumented indentation data obtained with pointed indenters. J. Phys. D. Appl. Phys. **41**(21), 215407 (2008)
6. E. Berkovich, Three-faceted diamond pyramid for micro-hardness testing. Ind. Diam. Rev. **11**(127), 129 (1951)
7. W.C. Oliver, G.M. Pharr, Improved technique for determining hardness and elastic modulus using load and displacement sensing indentation experiments. J. Mater. Res. **7**(6), 1564 (1992)
8. W.C. Oliver, G.M. Pharr, Measurement of hardness and elastic modulus by instrumented indentation: Advances in understanding and refinements to methodology. J. Mater. Res. **19**(1), 3 (2004)
9. Z.-H. Xu, X. Li, Effect of sample tilt on nanoindentation behaviour of materials. Philos. Mag. **87**(16), 2299 (2007)
10. J.D. Ellis, S.T. Smith, R.J. Hocken, Alignment uncertainties in ideal indentation styli. Precis. Eng. **32**(3), 207 (2008)
11. M. Saket Kashani and V. Madhavan: The effect of surface tilt on nanoindentation results, in Volume 10: Mechanics of Solids and Structures, Parts A and B (Proc. of the ASME, International Mechanical Engineering Congress and Exposition. Seattle, WA, USA 2007, 1067 (2007)
12. M.S. Kashani, V. Madhavan, Analysis and correction of the effect of sample tilt on results of nanoindentation. Acta Mater. **59**(3), 883 (2011)
13. H. Huang, H. Zhao, C. Shi, L. Zhang, Using residual indent morphology to measure the tilt between the triangular pyramid indenter and the sample surface. Meas. Sci. Technol. **24**(10), 105602 (2013)
14. C. Shi, H. Zhao, H. Huang, L. Xu, L. Ren, M. Bai, J. Li, X. Hu, Effects of indenter tilt on nanoindentation results of fused silica: an investigation by finite element analysis. Mater. Trans. **54**(6), 958 (2013)
15. A. Leitner, V. Maier-Kiener, D. Kiener, Extraction of flow behavior and Hall-Petch parameters using a nanoindentation multiple sharp tip approach. Adv. Eng. Mater. **19**(4), 1600669 (2017)
16. G. Kermouche, J.L. Loubet, J.M. Bergheau, Extraction of stress–strain curves of elastic–viscoplastic solids using conical/

pyramidal indentation testing with application to polymers. Mech. Mater. **40**(4), 271 (2008)

17. D.J. Morris, A.M. Vodnick, R.F. Cook, Radial fracture during indentation by acute probes II: experimental observations of cube-corner and Vickers indentation. Int. J. Fract. **136**(1), 265 (2005)
18. I. M. Gelfand and T. Alekseyevskaya (Gelfand): in *Geometry*, edited by I. M. Gelfand and T. Alekseyevskaya (Gelfand) (Springer New York, New York, NY, 2020), pp. 231–401.
19. J.E. Jakes, R.S. Lakes, D.S. Stone, Broadband nanoindentation of glassy polymers: Part II Viscoplasticity. J. Mater. Res. **27**(02), 475 (2012)
20. H. Chakraborty, A. Sinha, N. Mukherjee, D. Ray, and P. Protim Chattopadhyay: A study on nanoindentation and tribological behaviour of multifunctional ZnO/PMMA nanocomposite. *Mater. Lett.* **93**, 137 (2013).
21. P. Jindal, M. Sain, N. Kumar, Mechanical characterization of PMMA/MWCNT composites under static and dynamic loading conditions. Mater. Today Proc. **2**(4), 1364 (2015)
22. T. Jin, X. Niu, G. Xiao, Z. Wang, Z. Zhou, G. Yuan, X. Shu, Effects of experimental variables on PMMA nano-indentation measurements. Polym. Test. **41**, 1 (2015)
23. I.N. Sneddon, Relation between load and penetration in axisymmetric Boussinesq problem for punch of arbitrary profile. Int. J. Eng. Sci. **3**, 47 (1965)
24. J.E. Jakes, Improved methods for nanoindentation Berkovich probe calibrations using fused silica. J. Mater. Sci. **53**(7), 4814 (2018)
25. A. F. Yee and M. T. Takemori: Dynamic bulk and shear relaxation in glassy polymers. I. Experimental techniques and results on PMMA. *J. Polym. Sci. Polym. Phys. Ed.* **20**(Copyright 1982, IEE), 205 (1982).
26. J. Schindelin, I. Arganda-Carreras, E. Frise, V. Kaynig, M. Longair, T. Pietzsch, S. Preibisch, C. Rueden, S. Saalfeld, B. Schmid, J.-Y. Tinevez, D.J. White, V. Hartenstein, K. Eliceiri, P. Tomancak, A. Cardona, Fiji: an open-source platform for biological-image analysis. Nat. Methods **9**(7), 676 (2012)

Supplemental information for:

Contact area correction for surface tilt in pyramidal nanoindentation

Joseph E. Jakes[1*] and Douglas Stauffer[2]

[1]Forest Biopolymers Science and Engineering, USDA Forest Service, Forest Products Laboratory. One Gifford Pinchot Drive, Madison, Wisconsin, United States 53726.

[2]Hysitron Product Line, Bruker Nano Surfaces & Metrology, 9625 West 76th St, Eden Prairie, Minnesota, United States 55419.

*e-mail: joseph.e.jakes@usda.gov

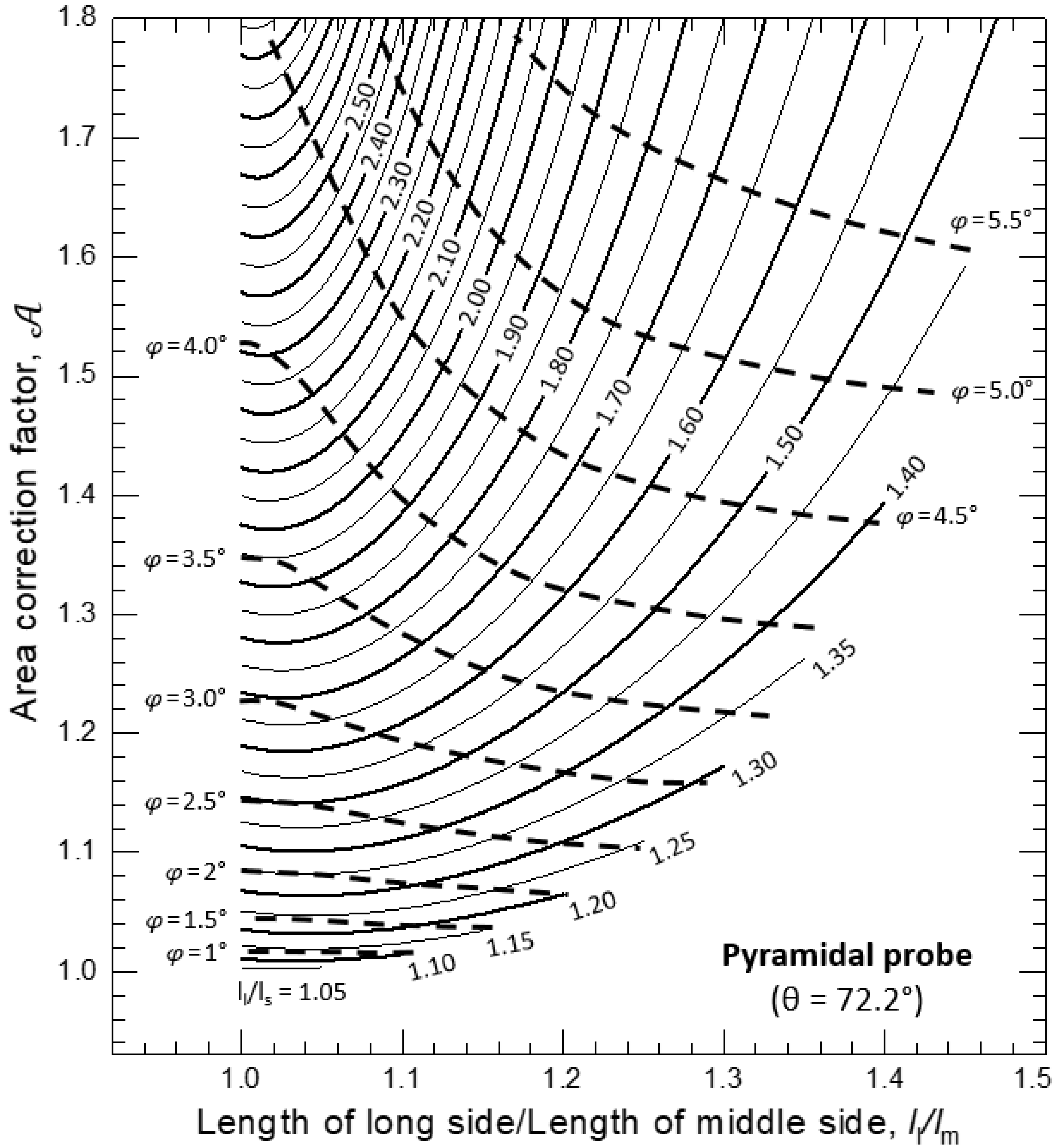

FIG. S1. Area correction factor ($\mathcal{A}$) contour plots for a pyramidal probe (θ = 77.2°). The $\mathcal{A}$ can be determined using the ratios of the longest side length to medium side length (l_l/l_m) and longest side length to shortest side length (l_l/l_s). The l_l/l_m is plotted on the abscissa, and the l_l/l_s values follow the solid line contours. The surface tilt φ angles are indicated as dashed line contours.

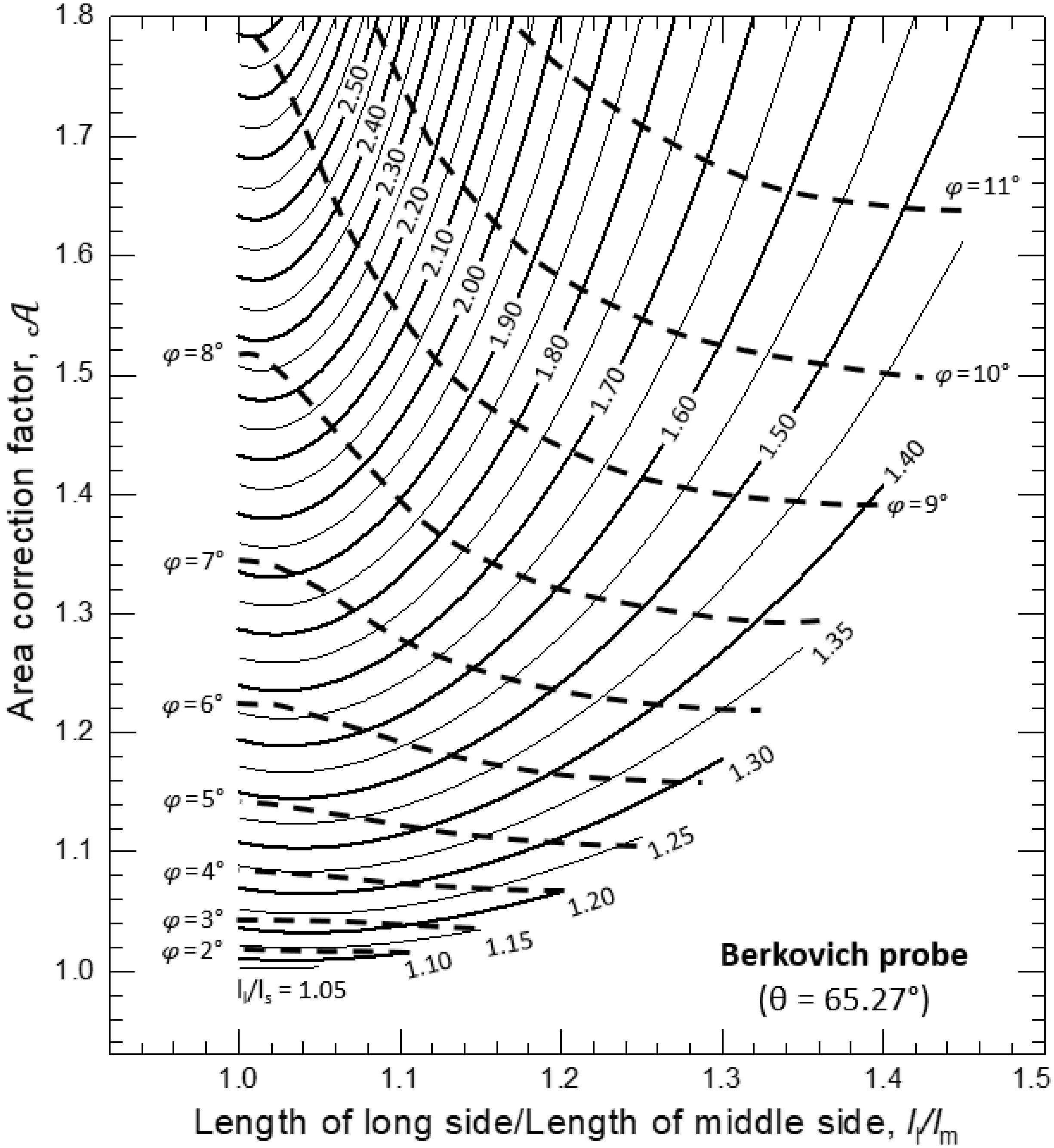

FIG. S2. Area correction factor ($\mathcal{A}$) contour plots for a Berkovich probe (θ = 65.27°). The $\mathcal{A}$ can be determined using the ratios of the longest side length to medium side length (l_l/l_m) and longest side length to shortest side length (l_l/l_s). The l_l/l_m is plotted on the abscissa, and the l_l/l_s values follow the solid line contours. The surface tilt φ angles are indicated as dashed line contours.

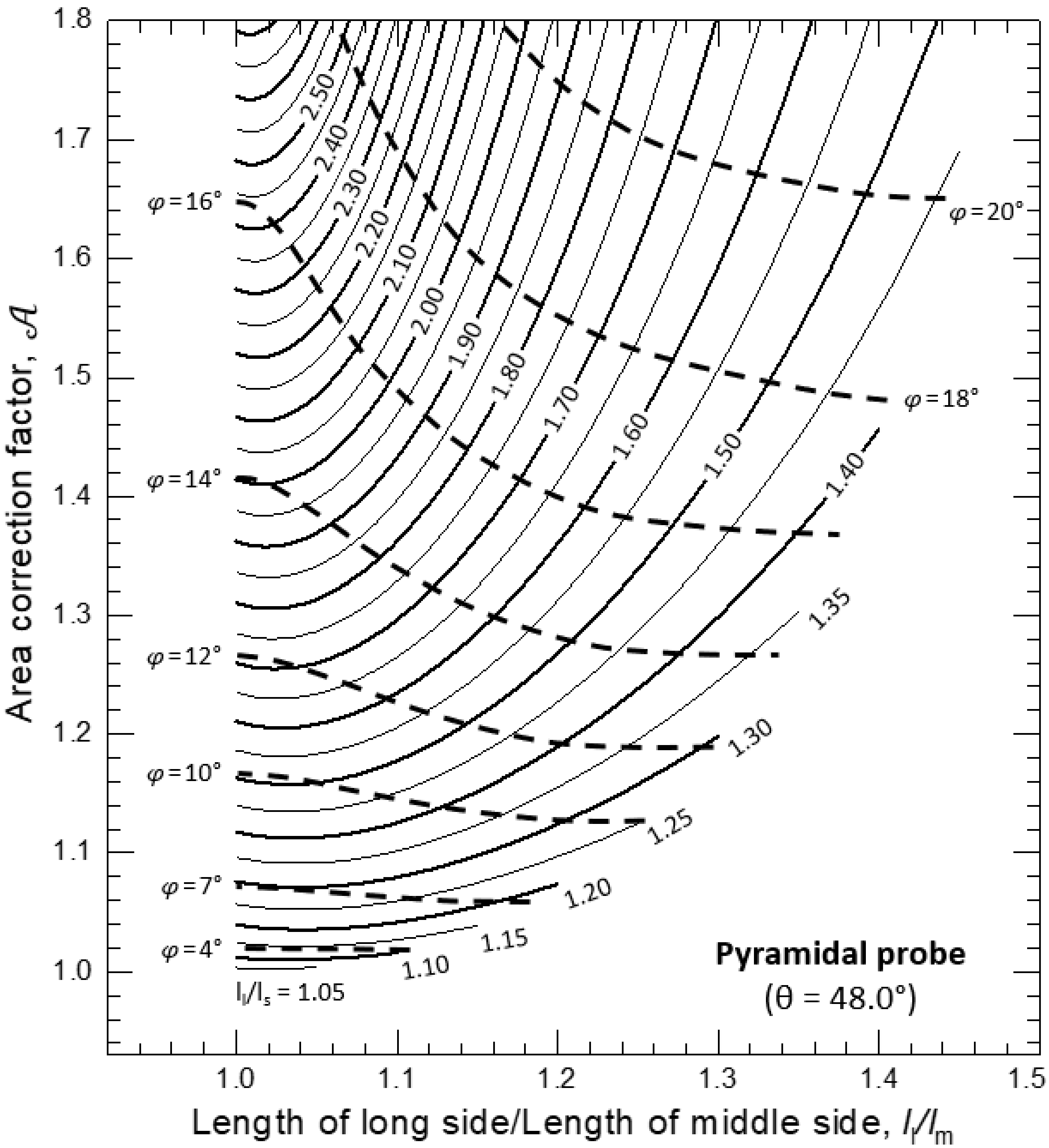

FIG. S3. Area correction factor ($\mathcal{A}$) contour plots for a pyramidal probe (θ = 48.0°). The $\mathcal{A}$ can be determined using the ratios of the longest side length to medium side length (l_l/l_m) and longest side length to shortest side length (l_l/l_s). The l_l/l_m is plotted on the abscissa, and the l_l/l_s values follow the solid line contours. The surface tilt φ angles are indicated as dashed line contours.

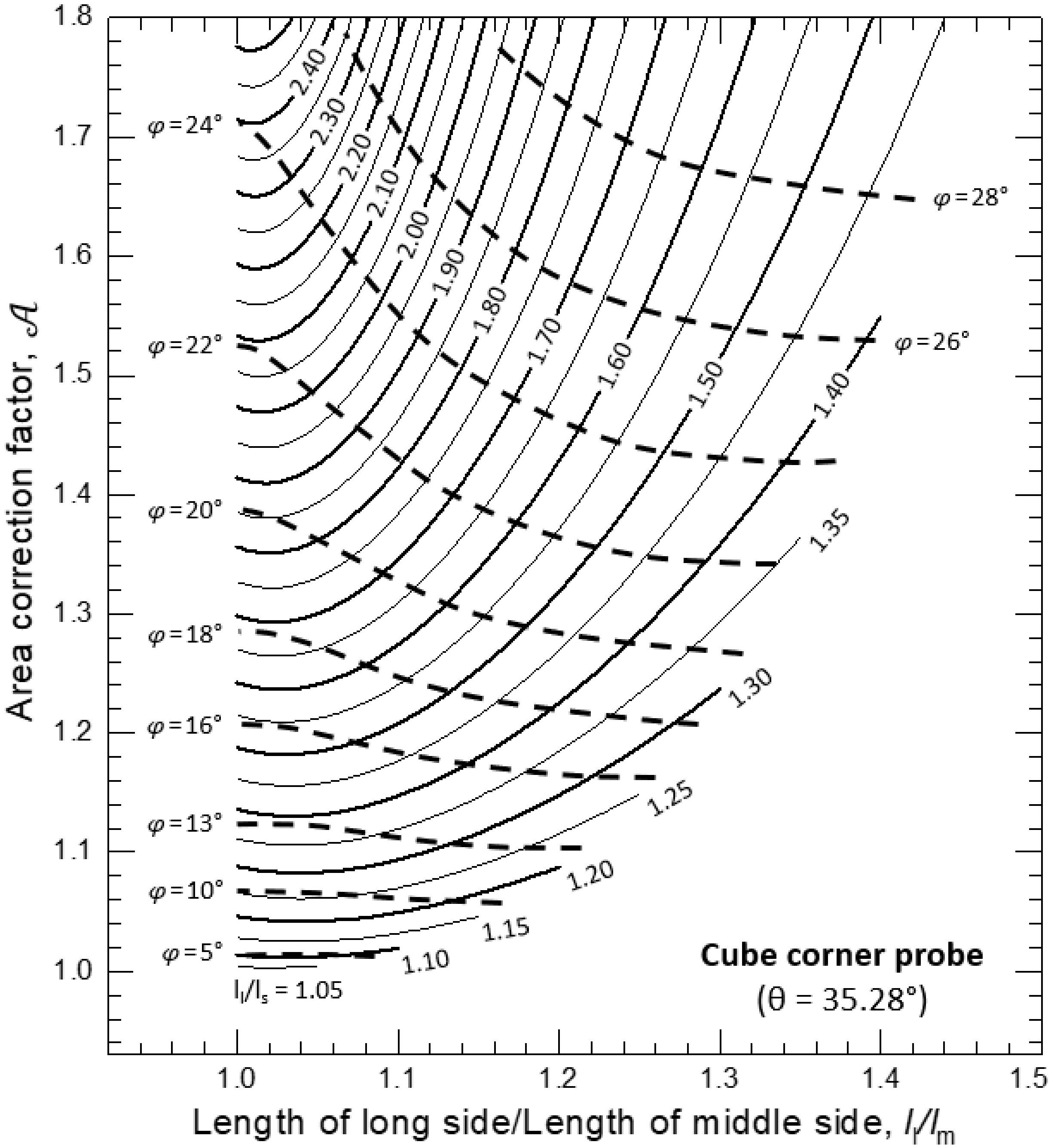

FIG. S4. Area correction factor ($\mathcal{A}$) contour plots for a cube corner probe (θ = 35.28°). The $\mathcal{A}$ can be determined using the ratios of the longest side length to medium side length (l_l/l_m) and longest side length to shortest side length (l_l/l_s). The l_l/l_m is plotted on the abscissa, and the l_l/l_s values follow the solid line contours. The surface tilt φ angles are indicated as dashed line contours.